Supplementary information

Renewable synthetic crude oil to mitigate carbon emissions and fossil fuel dependency

Hidde Kolmeijer,[a,b] Juan D. Medrano-García ,[a,b] Abhinandan Nabera,[a,b] and Gonzalo Guillén-Gosálbez*[a,b]

[a] *Institute for Chemical and Bioengineering, Department of Chemistry and Applied Biosciences, ETH Zurich, Vladimir Prelog Weg 1, Zurich 8093, Switzerland.*

[b] *NCCR Catalysis, Zurich 8093, Switzerland.*

* *Corresponding author. Email: gonzalo.guillen.gosalbez@chem.ethz.ch*

Table of contents

Tables and figures

1. A brief historic background

The Fischer-Tropsch (FT) process, developed in Germany in the 1920s, converts synthesis gas into liquid hydrocarbons. Its invention was motivated by concerns over energy security, as the country lacked large petroleum reserves. During World War II, FT-plants were built at scale to produce synthetic fuels from coal, meeting a large share of Germany's transport fuel needs despite allied blockades.[1] The technology proved capable of delivering drop-in fuels compatible with existing engines and infrastructure, laying the foundation for its later adaptation in other contexts. However, in the post-war period, low-cost crude oil and the rise of conventional refining reduced the role of the FT-process in most industrialised nations.[2]

The process regained prominence in the second half of the 20th century in South Africa, where geopolitical circumstances again made energy security a priority. During the apartheid era, international sanctions and embargoes sharply restricted crude oil imports. Sasol, the state-backed energy company, turned to coal-to-liquid (CTL) FT-synthesis to secure domestic fuel supplies.[3] Through decades of operation, Sasol scaled the technology to unprecedented capacities, operating the largest FT-facilities in the world. These plants proved the durability, scalability, and commercial viability of the process over sustained periods, establishing it as a mature, high-TRL (technology readiness level) industrial process capable of competing with petroleum refining when economic or political conditions made it necessary.[4]

In subsequent decades, the focus of FT-development shifted towards cleaner fossil feedstocks, particularly natural gas. The Shell Middle Distillate Synthesis (MDS) emerged as a significant commercial application, allowing for the conversion of fossil methane into high-value middle distillates such as naphtha, kerosene, and diesel.[5] The first MDS plant, commissioned in Bintulu, Malaysia in 1993, demonstrated that FT-process could operate continuously on natural gas at full commercial scale while producing fuels meeting mandatory industry specifications.[6] Building on this success, Shell developed the Pearl gas-to-liquid (GTL) plant in Qatar, the largest FT facility to date. This investment allowed for the monetisation of large natural gas reserves, converting it to valuable hydrocarbon products.[7]

More recently, FT-based processes have been explored for low-carbon fuels and chemicals from renewable carbon feedstocks.[8,9] Accordingly, our work assesses the economic and technical barriers of a sustainable MDS economy, as shown in the main manuscript.

2. Process modelling

This section includes the resulting process models as used in this work. The structure of the section follows the same steps as the MDS. First, the generation of synthesis gas from all types of feedstocks will be discussed. This is followed by a section on the FT-process, converting syngas into syncrude. Finally, the downstream syncrude upgrading and process quality control will be discussed. We consider the production of 3.6 Mt of syncrude annually, equal to 480 tonnes per day. Each process was assumed to operate all year round, resulting in 8760 hours per year. The following section will describe the process flowsheets and operating conditions for each type of feedstock, the FT-process, and the downstream refining and upgrading. The energy balance for each pathway was solved using Aspen Energy Analyzer, yielding the overall heating and cooling duties by designing the heat exchange network (HEN). The overall mass balance for each process is summarised in the respective section. In all Aspen HYSYS simulations, *i.e.*, excluding the biomass gasification, the SRK fluid package was used.

2.1. Feedstock conversion

This work includes several sustainable feedstocks, each suitable to generate synthesis gas (CO and H_2 in a molar ratio 1:2):

- Biomass, separated into two categories, agricultural and forestry residues. The gasification of biomass was simulated in Aspen Plus v12.
- Biogas, consisting of methane and carbon dioxide in molar ratio 1:1. For biogas, the bi-reforming reactor was modeled in Aspen HYSYS v12.
- DAC CO_2 and green hydrogen, converted to syngas in a reverse water gas shift (RWGS) reactor.

2.1.1. Biomass gasification

The process simulation of biomass to synthesis gas was adapted from the literature.[10] The process was modeled in Aspen HYSYS v12 and the process flowsheet for both agricultural waste and forestry residues is shown in **Fig. S1**. The NRTL fluid package, using the Redlich-Kwong equation of state was used. To address the diversity of biomass sources within both categories, two benchmark products were chosen to simplify the process. For agricultural residues, wheat straw was chosen as a benchmark product. For forestry residues, the feedstock is modelled as birch tree. These feedstocks were selected as proxies for all biomass types, as their composition is representative of the average biomass composition and simplifies the Aspen HYSYS simulations required. The proximate, ultimate, and sulphur analyses for both feedstocks can be found in **Tables S1** and **S2**. The simulation is based on previous work by Medrano-García *et al.*[10] The biomass was assumed to be gasified at 700 °C, producing gaseous products and biochar. The biochar was modelled to be combusted in the presence of oxygen, recovering heat and producing a pure stream of carbon dioxide to be prepared for storage by compressing at 110 bar. The syngas was purified, removing sulphur and excess water. A full description of each step can be found in the underlying literature.

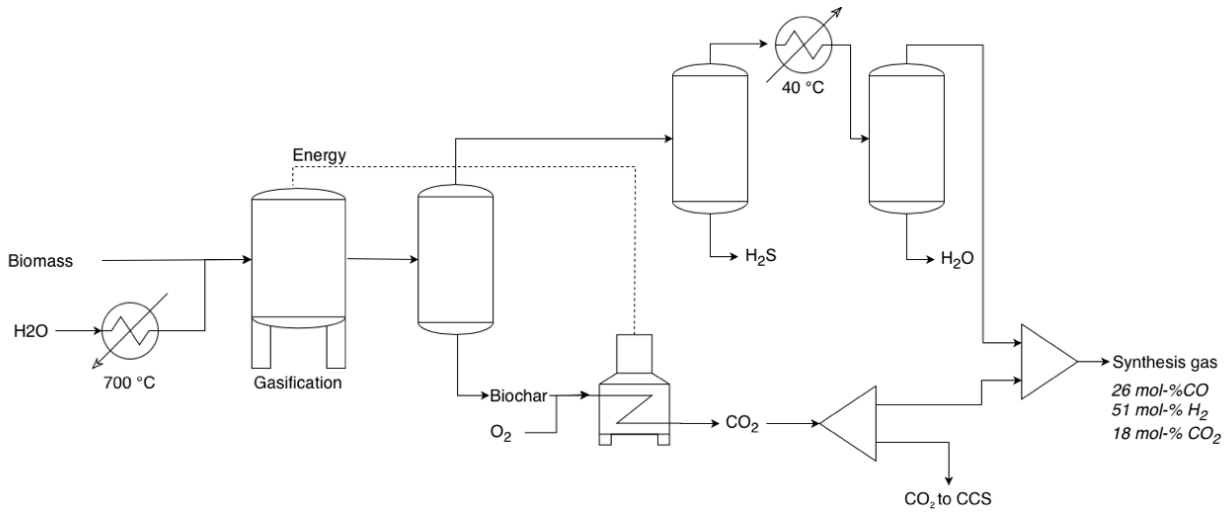

Fig. S1. Aspen Plus flowsheet for the gasification of agricultural and forestry biomass residues.

Table S1. Birch bark (forestry biomass) proximate, ultimate, and sulphur analyses, as adapted from Medrano García *et al*.[10]

Component	Proximate analysis (%)	Ultimate analysis (%)	Sulphur analysis (%)
Moisture	8.40	–	–
Fixed carbon (FC)	19.43	–	–
Volatile matter (VM)	78.49	–	–
Ash	2.07	2.07	–
Carbon	–	55.82	–
Hydrogen	–	6.56	–
Nitrogen	–	0.49	–
Chlorine	–	-	–
Sulphur	–	0.10	–
Oxygen	–	34.96	–
Pyritic	–	-	–
Sulphate	–	-	0.10
Organic	–	-	–

Table S2. Wheat straw (agricultural biomass) proximate, ultimate, and sulphur analyses, as adapted from Hasnain *et al.*[11]

Component	Proximate analysis (%)	Ultimate analysis (%)	Sulphur analysis (%)
Moisture	10.40	–	–
Fixed carbon (FC)	16.30	–	–
Volatile matter (VM)	67.20	–	–
Ash	6.40	6.40	–
Carbon	–	49.40	–
Hydrogen	–	6.10	–
Nitrogen	–	0.70	–
Chlorine	–	–	–
Sulphur	–	0.17	–
Oxygen	–	43.60	–
Pyritic	–	–	–
Sulphate	–	–	0.17
Organic	–	–	–

Table S3. Overall mass balance for the gasification of biomass from agricultural waste, for which wheat straw was assumed to be the benchmark feedstock.

Biomass gasification (agriculture)		
Input	**Value**	**Unit**
Wheat straw	2.85	kt per hr
Steam	0.23	kt per hr
Output	**Value**	**Unit**
Synthesis gas	2.36	kt per hr
Carbon monoxide	*37.5*	*wt.%*
Hydrogen	*6.14*	*wt.%*
Carbon dioxide	*52.1*	*wt.%*
Water	0.43	kt per hr

Table S4. Overall mass balance for the gasification of biomass from forestry residues, for which birch tree was assumed to be the benchmark feedstock.

Biomass gasification (forestry)		
Input	**Value**	**Unit**
Birch	2.65	kt per hr
Water	0.23	kt per hr
Output	**Value**	**Unit**
Synthesis gas	2.41	kt per hr
Carbon monoxide	*42.3*	*wt.%*
Hydrogen	*6.21*	*wt.%*
Carbon dioxide	*41.7*	*wt.%*
Water	0.23	kt per hr

2.1.2. Biogas bi-reforming

The bi-reforming of biogas was modeled in Aspen HYSYS v12 using the Peng Robinson fluid package. The process flowsheet is shown in **Fig. S2.** Biogas, the typical product of an anaerobic digester, entered the system at 1 bar and 40 °C.[12] It was compressed to 30 bar and mixed with steam, also at 30 bar, before entering the bi-reforming system. The reformer was modelled assuming a Gibbs equilibrium reactor, operating at 30 bar and 950 °C.[13] The outlet product was cooled down to 40 °C to liquify most of the water, after which the gaseous fraction was sent to the FT-system.

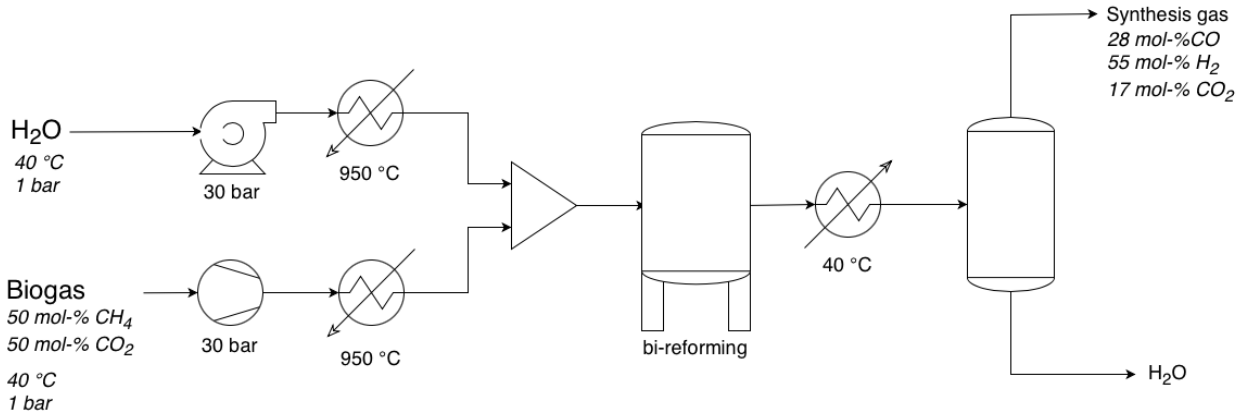

Fig. S2 Aspen HYSYS flowsheet for the bi-reforming of biogas.

Table S5. Overall mass balance for the generation of syngas from biogas, which was assumed to be a mixture of 50 mol% methane and 50 mol% carbon dioxide.

Biogas reforming		
Input	**Value**	**Unit**
Biogas	2.00	kt per hr
Steam	1.69	kt per hr
Output	**Value**	**Unit**
Synthesis gas	2.38	kt per hr
Carbon monoxide	*46.4*	*wt.%*
Hydrogen	*6.72*	*wt.%*
Carbon dioxide	*45.5*	*wt.%*
Water	1.32	kt per hr

2.1.3. Carbon capture and utilisation (CCU)

For the CCU-route, CO_2 and H_2 were taken as feedstock without further upstream process modeling. **Fig. S3** shows the flowsheet of this route up to the FT-reactor. Based on literature data, CO_2 was assumed to enter the system from a direct air capture (DAC) plant at 1 bar and 100 °C.[14] For hydrogen, the inlet flow was assumed to be derived from a proton exchange membrane (PEM) water electrolysis system, operating at 30 bar and 70 °C.[15] This means that for both feedstocks, prior heating was required, as shown in **Fig. S3**. For DAC CO_2, additional compression was also needed up to 30 bar. To then yield H_2 and CO in molar ratio 1:1, a reverse water gas shift (RWGS) reactor was included prior to the FT-system. Again, a Gibbs equilibrium reactor was used to model the reaction, here operating at 30 bar and 800 °C.[16] The gaseous product mixture was cooled down to 70 °C to separate most of the water formed. The vapour product was sent to the FT-reactor inlet.

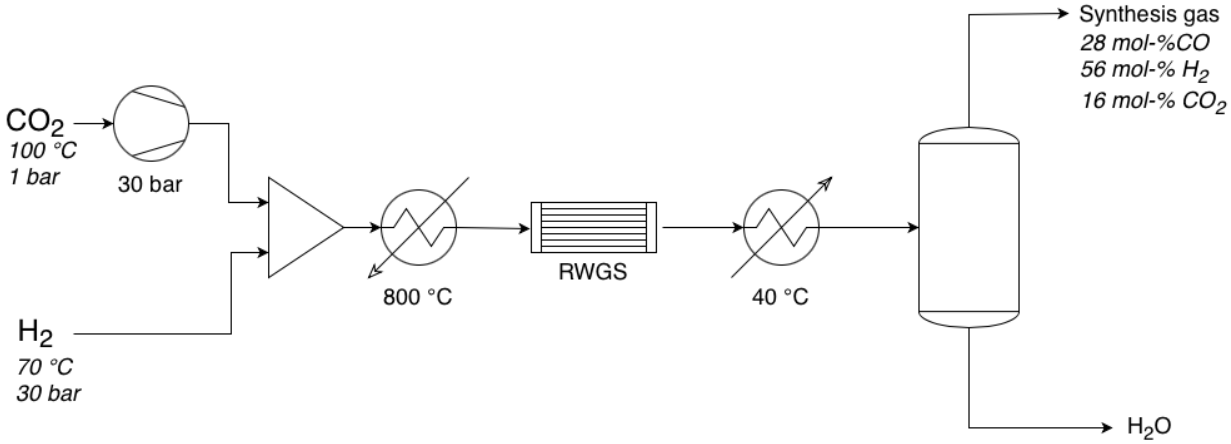

Fig. S3. Aspen HYSYS flowsheet for generation of synthesis gas from DAC CO_2 and green hydrogen from PEM water electrolysis.

Table S6. Overall mass balance for production of syngas in the CCU route, utilising CO_2 sequestered from the atmosphere using DAC and green hydrogen from a PEM electrolyser. Part of the CO_2 required for the RWGS reactor was supplied by recycling the outlet stream from the oxy-combustion unit. This recycle stream reduced the need for fresh CO_2 input and consequently lowered the associated DAC cost.

CO_2 capture and utilisation (CCU)		
Input	**Value**	**Unit**
DAC CO_2	1.72	kt per hr
Hydrogen	0.23	kt per hr
Recycled flue gas	1.46	kt per hr
Carbon monoxide	*0.13*	*wt.%*
Water	*0.08*	*wt.%*
Carbon dioxide	*0.79*	*wt.%*
Output	**Value**	**Unit**
Synthesis gas	2.61	kt per hr
Carbon monoxide	*49.8*	*wt.%*
Hydrogen	*7.2*	*wt.%*
Carbon dioxide	*43.0*	*wt.%*
Water	0.83	kt per hr

2.2. Fischer-Tropsch

The syngas, regardless of its feedstock source, was then converted to syncrude in a FT-reactor. This work assumes a low-temperature system (LTFT), which utilises an iron-based catalyst and operates at 30 bar and 230 °C.[17] This means the syngas inlet temperature was either heated or cooled down, depending on the type of feedstock. The composition of the FT-syncrude, as assumed in this work, can be seen in **Fig. S4**. The product distribution is based on publicly available industry data and the work by De Klerk.[18] The FT-reactor was followed by a syncrude distillation unit (sCDU), which operates equally to conventional refinery distillation columns. Both the FT reactor and the sCDU modelled in Aspen HYSYS v12 (**Fig S4**). For the sCDU, the Refining short-cut Column unit operation, already present in Aspen HYSYS, was used. In order to model the FT process, we defined the main products using their typical boiling point range: LPG, naphtha, kerosene, diesel, and hydrowax. For these main products, the relevant properties (freeze point, density, cetane number, and aromatics content) were compared to industry specifications. The same was done for a linear blend of CDU fractions and the cracked hydrowax products, as discussed in the next section. Note that costs and emissions are mostly reported for 1 kg of syncrude oil. However, we model as well the downstream operations until the final products (*i.e.*, naphtha, kerosene, and diesel) to confirm the feasibility of the overall approach. Feasibility is therefore evaluated by confirming that specifications on final products can be met in the process simulation.

In the FT modelling framework, the key parameter governing conversion was the H_2/CO ratio, which was maintained at 2 across all feedstock routes. While the syngas composition varied in CO_2 content, only CO and H_2 participated in hydrocarbon formation, and CO_2 was treated as an inert species that passed through the reactor. A portion of this CO_2, together with light hydrocarbons from the reactor outlet, was routed to the oxy-combustion unit, where it was recovered as a concentrated CO_2 stream. This recycle reduced the requirement for fresh CO_2 feed, thereby lowering the associated cost of direct air capture. Alternatively, CO_2 could be removed upstream using a pre-reactor absorption step (*e.g.*, methyl ethyl amine; MEA), which would reduce gas throughput and reactor sizing but introduce additional capital and operating costs. An alternative process flowsheet regarded this option and indicated that either approach has a negligible effect on syncrude yields, downstream product specifications, and overall system performance. Life-cycle inventories and techno-economic results were generated independently for each feedstock to ensure a consistent and transparent basis for comparison.

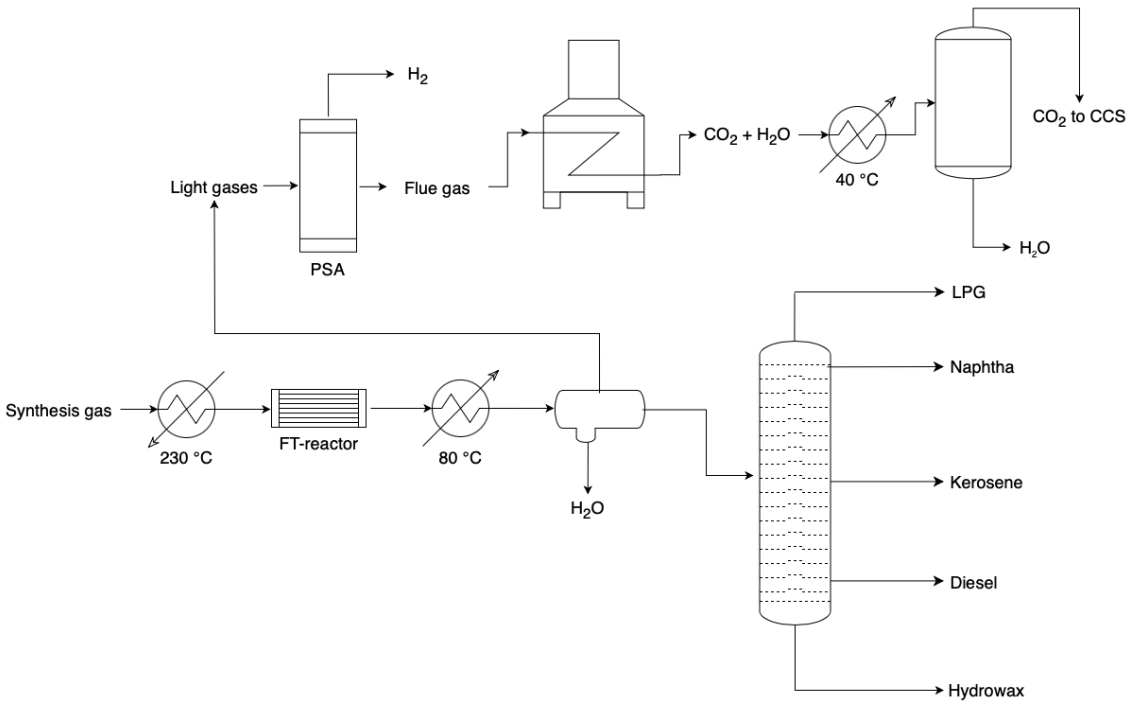

Fig. S4. Aspen HYSYS flowsheet for production of FT-syncrude from synthesis gas, including flue gas separation and combustion. The water produced in the FT-process is separated in a decanter, after which the light gases are combusted and the syncrude separated in a distillation column (sCDU), using the Aspen HYSYS refining short-cut column.

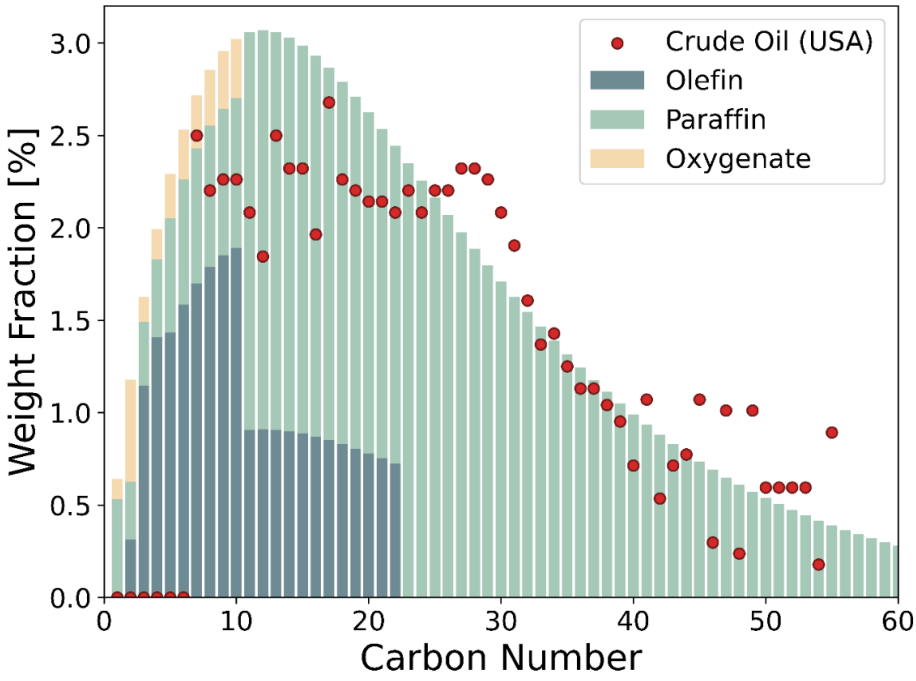

Fig. S5. Fischer-Tropsch product mixture as adapted from De Klerk.[18] The data was compared to the average composition of a barrel of crude oil, as indicated by the red dots.[19] Although the weight distribution is similar, further syncrude upgrading is still required for the products to meet industry specifications.

Table S7. Overall mass balance for the Fischer-Tropsch process, producing syncrude from syngas. Although the syngas inlet contained a significant fraction of CO_2, only CO and H_2 participated in the reaction. CO_2 was modelled as an inert species that passes through the FT reactor, consistent with its negligible reactivity on typical FT catalysts.

Fischer-Tropsch process		
Input	**Value**	**Unit**
Syngas	2.40	kt per hr
Output	**Value**	**Unit**
Syncrude	0.48	kt per hr
Water	0.64	kt per hr
Light process stream	1.28	kt per hr
Carbon dioxide	*83.5*	*wt.%*
Carbon monoxide	*9.5*	*wt.%*
Light hydrocarbons	*7.0*	*wt.%*

Table S8. Overall mass balance for the separation of FT-syncrude into the conventional petroleum fractions, separating water and light gases as well.

FT-syncrude separation		
Input	**Value**	**Unit**
Syncrude	0.480	kt per hr
Output	**Value**	**Unit**
LPG	0.018	kt per hr
Naphtha	0.069	kt per hr
Kerosene	0.044	kt per hr
Diesel	0.099	kt per hr
Hydrowax	0.249	kt per hr

2.3. Downstream upgrading

The specifications of the sCDU fuel outlet fractions as reported in Aspen HYSYS were compared to industry specifications on jet fuel and diesel.[20,21] As the FT-syncrude mainly consists of linear hydrocarbons, the low/temperature properties of the fuel fractions did not meet the specification yet. Therefore, the final step of the MDS consisted of the modelling of two cracking units in Aspen HYSYS v12. The hydrowax fraction coming from the sCDU was split into two fractions, where 90 wt.% was sent to the hydrocracker. Here, using the built-in Aspen HYSYS hydrocracking unit, the hydrowax was cracked at 130 bar and 205 °C.[22] The hydrogen requirement was met by the PSA outlet at the light gas separation (see **Section S2.2.**). The residual 10 wt.% was sent to a fluidised catalytic cracker (FCC) for further hydrowax upgrading. Operating at 3 bar and 200 °C, the FCC unit further enhanced the product specifications required for kerosene and diesel.[23] The subsystem, consisting of the hydrocracker and FCC, is visualised in **Fig. S6**. The hydrocracker and FCC unit were modelled using the built-in Aspen HYSYS refinery operation units, using a kinetic model. For this purpose, the inlet flow rate was converted to the kinetic lumps as specified in the model. More information on these process units can be found in the Aspen HYSYS user manuals.[24] The cost of this downstream section was calculated and is reported in the manuscript. However, it was not included in the comparison with the market price of crude oil, in order to maintain the same functional unit.

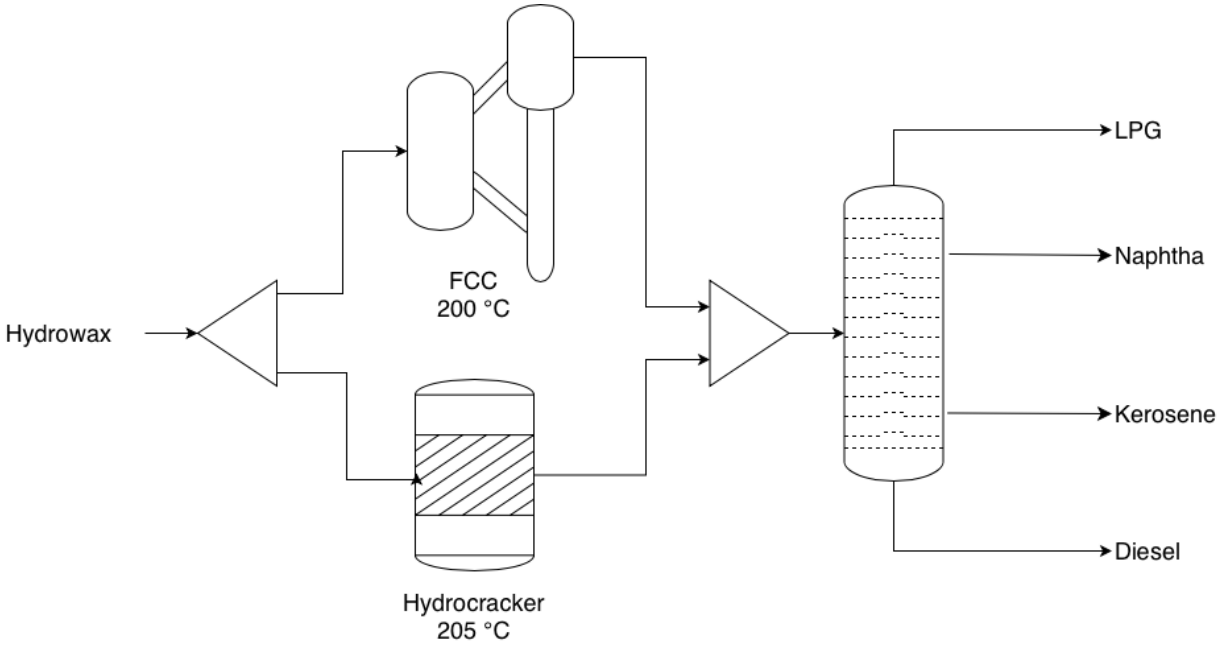

Fig. S6. Aspen HYSYS flowsheet for the upgrading of FT-hydrowax to valuable chemicals and fuels through catalytic and hydrocracking.

Table S9. Overall mass balance for the upgrading of FT-hydrowax into the conventional petroleum fractions at improved fuel properties

FT-hydrowax upgrading		
Input	**Value**	**Unit**
Hydrowax	0.250	kt per hr
Hydrogen	0.0045	kt per hr
Output	**Value**	**Unit**
LPG	0.033	kt per hr
Naphtha	0.071	kt per hr
Kerosene	0.093	kt per hr
Diesel	0.220	kt per hr
Other products	0.062	kt per hr

3. Feedstock availability

Literature data on biogas and biomass potential was gathered to account for their limited availabilities. These values were compared to the demand of crude oil for each country, shown in **Table S3**. The biomass and biogas availabilities are provided in **Tables S4** and **S5**. The syncrude potential from these sources (in million barrels per year) are provided in **Table S6**, facilitating a comparison with the crude oil demands from **Table S3**. For biomass, recent work by Huo *et al.* was used to aggregate data into agricultural and forestry residues for each of the selected regions. For biogas, the potential was taken from various sources, all listed in **Table S5**.

Carbon capture and utilisation (CCU) is virtually unbounded from the viewpoint of raw materials, as it merely depends on the amount of CO_2 in the atmosphere and the amount of water suited for electrolysis (assuming availability of the associated resources). However, CCU infrastructure might become a bottleneck due to the large amounts of renewable power required for green hydrogen production. Although DAC could be deployed on a gigatonne-scale, large-scale instalment would come at an increasingly high cost.[25] Moreover, green hydrogen demand in 2050 could rise to around 500 Mtpa, a similar scale to what would be required under this work's syncrude economy (~860 Mtpa).[26]

For crude oil, the demands as shown in **Table S3** were used as an upper limit on the availability. The petrochemical industry operates globally, with oil reserves limited to a number of countries. This means that, in order to meet primary energy demand, some countries rely on imports from oil producing countries.

Table S10. Domestic crude oil demand for the regions and countries included in this work.[27]

Region	Unit	Demand
Europe (EU+UK)	Million bbl per day	10.50
North America	Million bbl per day	21.00
China	Million bbl per day	16.00
Russia	Million bbl per day	3.60
India	Million bbl per day	5.20
Brazil	Million bbl per day	2.90
South Africa	Million bbl per day	0.60
Japan	Million bbl per day	5.60

Table S11. Biomass availability for each region or country included in this work. The input data was taken from Huo *et al.*[28], assuming the average aggregated availabilities.

Region	Unit	Agricultural Residues	Forestry Residues
Europe (EU+UK)	Mtpa	441.6	262.3
North America	Mtpa	833.0	286.9
China	Mtpa	688.1	124.7
Russia	Mtpa	122.7	123.7
India	Mtpa	802.7	38.2
Brazil	Mtpa	406.8	82.8
South Africa	Mtpa	56.8	18.4
Japan	Mtpa	15.7	28.7

Table S12. Biomethane availability for each region or country included in this work. The data was adapted from various literature sources, listed below as well.

Region	Unit	Biomethane availability	Source
Europe (EU+UK)	bcm	165.0	IEA[29]
North America	bcm	73.6	Dale *et al.*[30]
China	bcm	175.0	Li[31]
Russia	bcm	69.4	IEA bioenergy[32]
India	bcm	125.0	Dey and Thompson[33]
Brazil	bcm	50.8	CI Biogas[34]
South Africa	bcm	20.0	Marrison and Larson[35]
Japan	bcm	5.4	Yokohama and Matsumura[36]

Table S13. Maximum potential of syncrude from biogas and biomass in each region, calculated with the mass balances and feedstock availabilities presented in **Tables S11** and **S12**.

Region	Unit	Syncrude-forestry	Syncrude-agriculture	Syncrude-biogas
Europe (EU+UK)	Million bbl per day	1.0	1.7	2.5
North America	Million bbl per day	1.2	3.1	1.1
China	Million bbl per day	0.5	2.6	2.7
Russia	Million bbl per day	0.5	0.5	1.1
India	Million bbl per day	0.2	3.0	1.9
Brazil	Million bbl per day	0.3	1.5	0.8
South Africa	Million bbl per day	0.1	0.2	0.3
Japan	Million bbl per day	0.1	0.1	0.3

4. Assumptions and limitations of the study

- For the Aspen simulations, a MDS production plant with a capacity of 34 million barrels of syncrude per year was assumed. The modelled syncrude production was therefore of similar size to a conventional refinery.[37]
- Biomass was split into agricultural residues and forestry waste. The Aspen Plus simulations, as discussed in **Section S2.1**, assumed biomass input data representative for these two categories. For agriculture, the simulation assumed the gasification of wheat straw, whereas for forestry, birch bark was taken as a benchmark.[38] Our analysis on the ultimate, proximate, and sulphur analyses of various biomass types shows that, although different, the Aspen Plus simulations would on average lead to very similar syngas outlet compositions. Biomass types with larger fractions of hydrogen atoms will result in better chemical feedstocks, as hydrogen is the limiting factor in most biogenic syngas production processes.
- A ratio of 1:1 of methane and carbon dioxide was assumed for biogas. Typically, molar fractions for methane are between 50 and 75%, with the residual fraction consisting of carbon dioxide and various trace gases. A larger fraction of methane in the biogas would substantially improve the results, as it would yield results closer to existing simulations for FT-products from natural gas.
- For biogas generation, we consider a blend of several biogenic wastes as feedstocks. Based on work by Istrate *et al.*, biogas was assumed to be composed of manure, sequential crops, wastewater sludge, and agricultural residues.[12] The transport and storage of biogas were not included in the scope of this work.
- The availabilities of biogas and biomass were taken from separate sources, as discussed in **Section S3**. With the lack of well-defined system boundaries in the underlying data, the possibility of double accounting availabilities exists. To overcome this limitation, our work includes sensitivity analyses on cost, emissions, and availabilities. However, more research on scarce biogenic feedstocks and their implications in the economy will be required to come to finite conclusions on the economic impact of utilising large amounts of biogenic feedstocks.
- Industrial heating was assumed to be supplied through natural gas. Currently, refineries depend on sophisticated and optimised steam networks for process heating. To assess the consequence of a rapid transition to a syncrude economy, this system of fossil heating was assumed to remain in place. Therefore, no sustainable sources of process heating were included in this work.
- Specific to the process simulations in this work is that the lightest fraction from the syncrude CDU contains substantial amounts of CO_2, originating from the generation of syngas. For biomass gasification, biogas reforming, and the reverse water-gas shift reaction (using DAC-derived CO_2 and green hydrogen), the syngas in all simulations contains about 17 mol-% CO_2. Following the FT-synthesis and CDU separation, the CO_2-rich light hydrocarbon stream was assumed to be combusted with oxygen, producing a concentrated stream of CO_2 and heat that could be recovered for process integration. In the life-cycle assessment (LCA), this CO_2 stream was considered geologically stored,

thereby achieving permanent atmospheric removal. The mass and energy balances for the compression and storage of CO_2 were taken from an existing inventory, as described in **Section S6**.

- CO_2 removal was therefore assumed to occur after the FT process. Alternatively, the CO_2 present in the syngas at the FT reactor inlet could be separated using established technologies such as monoethanolamine (MEA) absorption. Our sensitivity analysis indicates that, in the case of biogas, this would add approximately 50-75 USD per tonne CO_2 (equivalent to 14-21 USD per bbl syncrude).[39] By allowing CO_2 to pass through the system, as assumed in this work, additional heating requirements of around 50 MJ per bbl syncrude were required, corresponding to 0.15 USD per bbl (see Fig. S4, where the syngas is heated to 230°C). While the larger gas streams increase CAPEX, the lower CAPEX in the reactor and upgrading sections when applying MEA absorption would not necessarily lead to a substantial reduction in overall costs. This is because (1) MEA absorption itself adds approximately 3 USD per bbl syncrude, and (2) total CAPEX (Fig. 2 in the main manuscript) is relatively small compared with other cost drivers such as feedstock prices and utilities. Consequently, leaving CO_2 in the syngas was found to provide a modest economic advantage.
- The blend of the product fractions leaving the sCDU and the output flows from the hydrowax upgrading steps were assumed to be blended on a linear basis. This means that properties such as freeze point and octane number are assumed to be a linear combination of the properties of the inlet streams to the blending pool. Although exhaustive studies exist on the blending of FT-products, a more detailed blending model was outside of the scope of this work. More importantly, crucial fuel properties such as density and cold properties were shown to correlate almost linearly with the amount of FT-products added.[40]
- The calculation of labour requirements for each type of syncrude are mostly based on the most recent available data, which is based on plants of average size. However, this work also includes several technologies which operate at a much smaller scale than the current petrochemical industry, such as DAC and green hydrogen production. For this reason, relatively high full-time equivalent (FTE) data is reported, as processes are currently not utilising their full economies of scale. As these technologies mature, larger, more efficient plants will be built. These higher productivities will yield lower FTE values per functional unit. A comprehensive social LCA would be required to capture these effects.
- The life cycle inventories for this study were derived from the ecoinvent database, applying the cut-off system model and can be found in **Section S6**. Relevant datasets were selected directly, without any modifications. A global system boundary was adopted, meaning that regional variations in the inventories were not taken into account.
- The life cycle assessment (LCA) calculations were done on a cradle-to-gate basis. For the gate, the assumption was made that it would include the production of syncrude. The total emissions to produce either syncrude or fossil crude were normalised over the production volume, to allow for a direct comparison. In a second assessment, the ecoinvent data on petroleum refining was used to calculate the environmental impact of naphtha, kerosene, and diesel (the right side of **Fig. 5** of the manuscript). The choice to use the ecoinvent database was used instead of the mass and energy balances computed

in this work was made in order to maintain a fair comparison between fossil and MDS-products. The MDS-process has been modelled to yield the same weight distribution of naphtha, kerosene, and diesel as conventional petroleum. Therefore, the mass-based allocation in ecoinvent would also be valid for the syncrude scenarios.

- The biogas and biomass transport contributions were excluded from this study, as a full supply chain analysis would be required and the climate impact is generally negligible. For example, assuming 50 km biomass transport using the 'transport, freight, lorry 16-32 t, EURO3' dataset from ecoinvent v3.10, the GWP 100 contribution amounts to 0.19 kg CO_2-eq. per ton-km, corresponding to only 0.05 kg CO_2-eq. per kg of syncrude produced.

5. Techno-economic analysis

The economic cost calculation consists of two categories: capital expenditure (CAPEX) and operational expenditure (OPEX). This section provides a full description of the calculations for both. Input data for both CAPEX and OPEX was taken from the mass and energy balances, calculated through extensive process simulations. The overall mass balances were already reported in **Section S2**, the inventories including the energy balance are shown in **Section S6**, covering life cycle assessment. The processes were modelled at scales representative for the (petro)chemical industry, therefore falling within the validity ranges of the costing models used.

5.1. Capital expenditure

The capital cost calculations presented in this section are based on the work by Onel *et al.*[41] Standard approaches compute first the purchase costs of the units from their capacities and derive the total CAPEX using multiple factors. Here we use instead aggregated correlations that are based on the plant capacity. Specifically, the economic calculations for all processes are based on non-linear literature correlations, each describing the inside battery limits (IBL) cost for a specific process unit or whole production site. The correlations are typically of the form shown in **Equation S1**.

$$C_i = \left(\frac{S}{S_0}\right)^n \cdot C_0 \qquad \textbf{(Equation S1)}$$

where:

- S is the required production scale;
- S_0 is the reference scale;
- C_0 is the cost at S_0;
- n is the scaling exponent;
- S_{max} is the upper value for which the correlation is valid.

The total capital cost for a certain production route was calculated as the sum of all process contributions. Following the original work, the total plant costs (TPC) is computed from the sum of the unit costs above considering the balance of plant cost (BOP), often 20% of the above cost that is added to account for additional necessary expenditures to run the plant (*e.g.*, utility plants).[41] Additionally, indirect costs (IC), accounting for engineering, are included, which adds a factor of 32%. The calculation of the TPC is reflected in **Equation S2**.

$$TPC = \sum_i C_i \cdot (1 + BOP) \cdot (1 + IC) \qquad \textbf{(Equation S2)}$$

where:

- C_i is the 2023 inside battery limits cost of a given process i;
- BOP is the balance of plant, an estimate of the total outside battery limits expenditures.
- IC are the indirect costs, and estimate of engineering start-up, royalties, and other factors.

The resulting cost for each process was originally calculated for 2014. To account for developments in capital investments, the Chemical Engineering Plant Cost Index (CEPCI) was used to correct the values to 2023.

$$TPC_{2023} = TPC_{2014} \cdot \frac{CEPCI_{2023}}{CEPCI_{2014}} \quad \textbf{(Equation S3)}$$

where:

- TPC_{2023} is the total 2023 cost;
- TPC_{2014} the total 2014 cost, calculated through **Equation S2**;
- $CEPCI_{2023}$ the 2023 Chemical Engineering Plant Cost Index;
- $CEPCI_{2014}$ the 2014 Chemical Engineering Plant Cost Index.

Finally, the total fixed capital cost (FCC) was annualised to account for investment financing (**Equation S4**).

$$TAC = ACCR \cdot TPC + OPEX \quad \textbf{(Equation S4)}$$

where:

- TAC is the total annualised capital cost;
- TPC is the fixed capital cost in 2023;
- ACCR is the annual capital charge ratio, derived from the interest rate and investment horizon;
- OPEX is the operational expenditure, as explained in the next section.

The ACCR was calculated assuming a fixed interest rate and investment payoff period (**Equation S5**).

$$ACCR = \frac{i \cdot (1+i)^n}{(1+i)^n - 1} \quad \textbf{(Equation S5)}$$

where:

- i is the interest rate;
- n is the number of years of compound interest.

The parameter values used for the calculation of CAPEX are shown in **Table S7** and **S8**. The processes included in this work and the respective source for the non-linear correlation of capital expenditure are schematically displayed in **Fig. S7**.

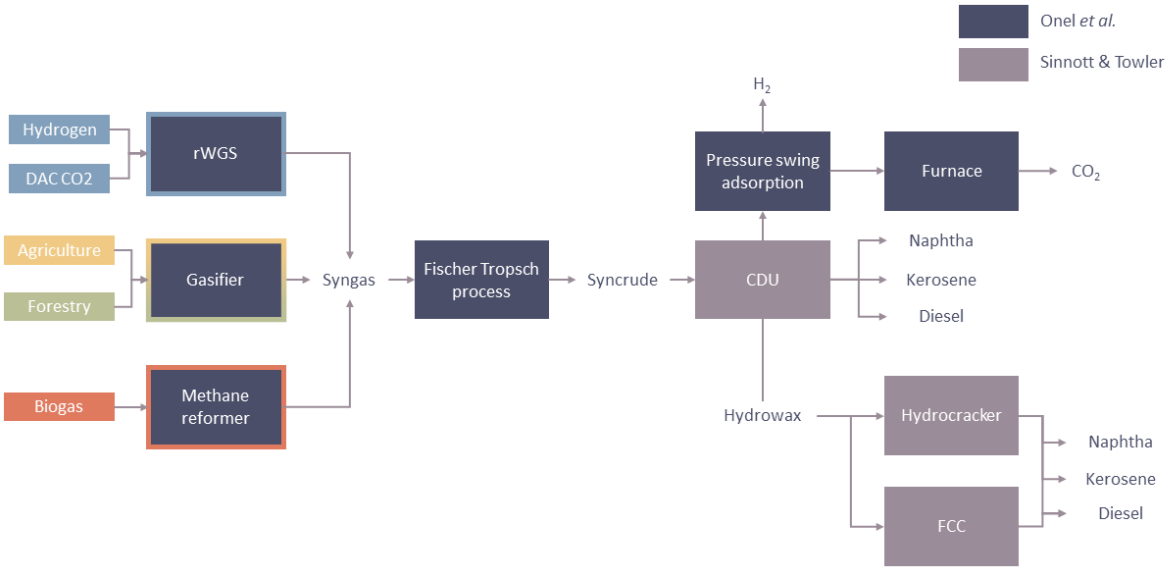

Fig. S7. Process included in the CAPEX calculations and the respective literature source.

Table S14. Capital Expenditure (CAPEX) input data. The mass balance data in kg feed per second were extracted from the mass balances (life cycle inventories and Aspen simulations). The input data for each process was adopted from Onel *et al.*[41] The data for the CDU, hydrocracker, and catalytic cracker was taken from Sinnott and Towler, but follows the same correlations as described in this section.[42]

Process	S	Unit	S_0	S_{max}	C_0 [2014 M$]	n	C [2014 M$]
Fischer-Tropsch process	666.7	kg/s	23.8	60.0	12.06	0.72	249.1
RWGS	867.4	kg/s	150.0	250.0	3.69	0.67	18.0
Biomass gasification	793.8	kg/s	17.9	-	60.00	1.00	2,660.8
Reforming unit	1,027.8	kg/s	12.2	35.0	30.22	1.00	2,545.8
Pressure swing adsorption	1.89	kmol/s	0.29	-	7.84	0.65	26.5
Crude distillation unit[42]	88,586.7	bpd	1.0	-	0.15	0.60	140.4
Hydrocracker[42]	44,247.1	bpd	1.0	-	0.20	0.60	121.4
Fluidised catalytic cracker[42]	4,916.3	bpd	1.0	-	0.21	0.60	34.5

Table S15. Operational data used for the TEA cost calculations.

Description	Value	Unit
Operating hours	8000	hr per yr
Interest rate[43]	10	%
Loan payback period	20	yr
ACCR	0.12	-
CEPCI 2014[44]	576.1	-
CEPCI 2023[44]	800.8	-
Balance of plant (BOP)[41]	0.20	-
Indirect costs (IC)	0.32	-

5.2. Operational Expenditure

The calculation of variable cost or OPEX included three factors:

- Feedstock cost.
- The cost of heating, cooling, and power duties, often referred to as utilities.
- The cost of labour and other fixed operational expenditures.

The cost of all feedstocks included in this work are listed in **Table S9**. As the objective of this work was to quantify the impact of rapidly deploying a syncrude economy, the feedstock costs all reflect current prices and do not include prospective results. For feedstocks, only a single global average value was assumed throughout this work due to the absence of reliable regional data.

The energy balance for each type of syncrude was assessed by solving the HEN in Aspen Energy Analyzer. To assess the cost of utility for each syncrude production route, the results from the compressor duties and the HEN were multiplied by the cost of electricity, heating from natural gas, and cooling water. Here, we assumed both global average costs, as well as regionalised data. This data can be found in **Table S10**.

Finally, for the labour cost for an industry which operate across the globe in a standardised matter, we assumed a single global average salary of 50,000 USD per year. Furthermore, this salary was assumed for workers in both the fossil petrochemical industry, as well as for workers in a syncrude-based economy. To calculate the labour costs, data on full-time-equivalence (FTE) was extracted from literature for each process. The FTE in hour per production unit data can be found in **Table S11**. This data was also used to calculate the required additional labour force for the deployment of large-scale syncrude production plants (**Table 1** in the main manuscript). No further aspects of the fixed OPEX were included in this work.

Table S16. Data on feedstock costs, including upper and lower bounds.

Name	Unit	Average	Lower	Upper
Hydrogen[45]	USD per kg	3.50	2.40	4.60
DAC CO_2[45]	USD per kg	0.12	0.09	0.39
Biogas[46]	USD per MMBtu	8.00	3.00	15.00
Wheat straw[47]	USD per tonne	70.00	40.00	100.00
Birch tree[48]	USD per tonne	45.00	30.00	80.00
Industrial oxygen[49]	USD per kg	0.30	0.20	0.40
Crude oil[50]	USD per bbl	77.00	60.00	90.00

Table S17. Utility cost data, including both regional and global average prices.

Region	Electricity [USD per kWh][51–53]	Heating [USD per MMBtu][54–56]	Cooling water [USD per GJ][57]
Europe (EU+UK)	0.12	12.50	-
North America	0.08	2.50	-
China	0.09	12.6	-
Russia	0.10	2.60	-
India	0.07	15.5	-
Brazil	0.11	26.4	-
South Africa	0.09	15.5	-
Japan	0.20	24.0	-
Global Average	0.10	7.00	0.38

Table S18. Full-time equivalent (FTE) data for each process. The data was used to calculate the additional labour requirements of a syncrude economy.

Process	Unit	FTE
Middle Distillate Synthesis (MDS)[58,59]	FTE per bpd*	$2.7 \cdot 10^{-4}$
PEM electrolysis[60]	FTE per kg hydrogen	$1.2 \cdot 10^{-6}$
Direct Air Capture (DAC)[61]	FTE per kg CO_2	$6.8 \cdot 10^{-7}$
Biomass Gasification[62]	FTE per kg biomass	$4.1 \cdot 10^{-6}$
Biogas reforming[63]	FTE per tonne biomethane	$7.9 \cdot 10^{-1}$

*Barrels per day.

6. Life cycle assessment (LCA)

6.1. Processes considered

The environmental impact of syncrude from various sources was calculated based on the process simulations as described in **Section 2**. The Aspen Plus and Aspen HYSYS simulations provided the mass and energy balances required for the generation of life cycle inventories (LCIs).

The functional unit used in the LCA calculations is shown in **Fig. S8**. The FT-process requires syngas as feedstock. The syngas can be produced by a portfolio of feedstocks, such as coal, natural gas, biogas, biomass, used plastics chemical recycling, or CO_2 captured from the atmosphere combined with hydrogen from electrolysis powered by renewable electricity. In our calculations, biogas-, biomass-, and CCU-based routes were assumed. For this purpose, biogas as a feedstock was assumed to be produced through the anaerobic digestion of biogenic waste material, such as industrial wastewater, sewage sludge, animal manure, agricultural residue crops, and sequential crops as done in previous works.[64] The exact blend composition and LCIs for biogas were directly adopted from the same literature source. Biomass was assumed to come from either agricultural waste or forestry residues. Electrolytic hydrogen is produced through water electrolysis in a PEM electrolyser using renewable energy (for example, onshore wind electricity in this work). CO_2 can be sequestered from the atmosphere through an adsorption-based technology, *i.e.*, direct air capture (DAC). Combining this CO_2 captured from air with hydrogen to produce chemicals and fuels is referred to as the carbon capture and utilisation (CCU) scenario.

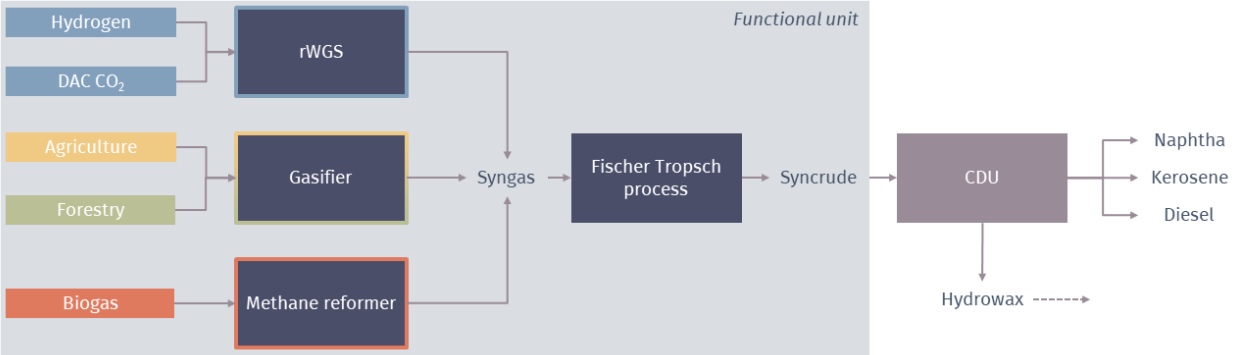

Fig. S8. Functional unit as chosen for the LCA calculations. All activities up to the production of 1 kg syncrude were included. The LCA calculations for the downstream upgrading and separation of the hydrocarbon products were based on the refinery operations taken from ecoinvent v3.10.

6.2. LCA calculations

We conduct an attributional life cycle assessment (LCA) following the ISO 14040 and 14044 standards.[65,66] This analysis is structured around the four standardised phases of LCA, as described below. The objective of our work is to evaluate the environmental performance of syncrude, in which renewable feedstock is utilised to substitute conventional fossil-based crude oil across the chemical and transportation sectors.

6.2.1. Goal and scope

The functional unit considered in this work is the total projected crude oil demand in 2025 across for a given regions, based on the market for petroleum. For this purpose, a cradle-to-gate system boundary was employed, encompassing all material and energy inputs, as well as associated up to 1 kg of syncrude. For the production of syncrude, all upstream inputs and outputs from the technosphere (*e.g.*, technosphere flows such as electricity) and the biosphere (*e.g.*, elementary flows such as CO_2 emissions) required for syncrude production are considered. To further assess the downstream effects of syncrude on the production of naphtha, diesel, and kerosene (the main components crude oil), we replace the existing fossil building blocks modelled in ecoinvent v3.10 with syncrude. In contrast to the techno-economic analysis, for the LCA calculations, the mass and energy balances from the ecoinvent database were used for the downstream refinery products (*i.e.*, naphtha, diesel, and kerosene), in order to present a fair comparison between both fossil and syncrude. This approach excludes the use phase of chemicals and fuels. The reason is that such use phase is assumed to be the same regardless of whether the products are manufactured via the business-as-usual process or the alternative FT one. Certainly, as the products leaving the refinery were modelled to match the properties of standard petrochemical products, a cradle-to-grave analysis would not change the comparison between syncrude and crude oil. The comparison was, therefore, made on a refinery basis. Furthermore, all calculations are based on global average assumptions.

6.2.2. Life cycle inventories

The life cycle inventories (LCIs) were employed using a combination of literature-based data and existing LCA databases. The downstream production of fossil naphtha, kerosene, and diesel in a refinery was modelled using the ecoinvent v3.10 database replacing crude oil in the market for petroleum with syncrude. For the production of syncrude, the mass and energy balances from the process simulations were used to generate process-specific inventories. These inventories included other market activities, either from the existing ecoinvent database or other literature. The inventories employed in this work are summarised in detail in **Tables S12** to **S16**.

To compute the LCIs, we apply the standard matrix-based formulation of LCA. The inventory vector *g* associated with the functional unit is derived from:

$$g = B \cdot A^{-1} \cdot f \qquad \textbf{(Equation S6)}$$

where *A* is the technosphere matrix, representing exchanges between economic activities; *B* is the biosphere matrix, linking those activities to environmental flows (*e.g.*, emissions, resource use); *f* is the final

demand vector, representing the functional unit (*i.e.*, the demand for petroleum in 2025); and *g* is the resulting inventory vector, quantifying all elementary flows required to satisfy the demand.[67] To model the syncrude and fossil crude systems within the LCA framework, we extend the background system matrices to include syncrude production pathways. Specifically, the technosphere matrix *A* and the biosphere matrix *B* are expanded to *A'* and *B'*, respectively. The additional rows and columns in *A'* represent the production routes for syncrude derived from renewable feedstocks (*e.g.*, biomass, biogas, CO_2 hydrogenation *via* CCU). Correspondingly, *B'* captures the associated environmental exchanges, including resource use and emissions linked to these pathways. This yields a modified inventory vector for the renewable syncrude system indirectly defossilising downstream products, *i.e.*, naphtha, diesel, and kerosene.

$$g' = B' \cdot A'^{-1} \cdot f \qquad \textbf{(Equation S7)}$$

This expansion enables the integration of syncrude-based supply chains into the background system, allowing the upstream substitution of fossil crude oil with renewable syncrude to propagate through the chemical and fuel production activities. The resulting modified inventory vector *g'* reflects the life cycle impacts of the syncrude system across all downstream products (naphtha, diesel, kerosene) derived from it. The choice for ecoinvent data for the downstream processes was made t ensure a direct comparison between these products and their fossil equivalents, as the Aspen HYSYS inventories would not include relevant factors such as integrated steam networks and refinery construction.

6.2.3. Life cycle impact assessment

The environmental impacts are assessed using midpoint and endpoint indicators. GHG emissions are quantified using 100-year global warming potential (GWP) from the IPCC 2021 assessment.[68] Additional endpoint categories, human health, ecosystems quality, and natural resource depletion, are evaluated using the ReCiPe 2016 v1.03 impact assessment method.[69] For a given inventory vector *g* or *g*', representing either the conventional or augmented system, the corresponding environmental impact vector *h* or *h*' is calculated as:

$$h' = Q \cdot g' \qquad \textbf{(Equation S8)}$$

Here, *Q* is the characterisation matrix that translates elementary flows into specific impact categories, based on the chosen LCIA method.

6.2.4. Interpretation

Finally, in the interpretation phase, we analyse the results as presented in the **Results and Discussion** section of the main manuscript. Not all LCA results are shown in the main manuscript. This section provides a full overview of the obtained results, including the risk of burden shifting. Specifically, the manuscript only describes the results for climate change. The environmental end points, human health, natural resources, and ecosystem quality are also relevant, particularly with regards to the potential occurrence of burden shifting, a theme often discussed when dealing with biogenic feedstock sources. **Tables S17**–**S20** show the numerical results for each type of syncrude and fossil crude on a cradle-to-gate basis, calculated in an equal manner to the results shown for climate change.

An uncertainty assessment of the scenarios was conducted using Monte Carlo sampling with 500 stochastically generated background datasets, derived from the ecoinvent Pedigree matrix. This matrix provides information on the uncertainty of LCI parameters based on lognormal distributions and the quality of the data available.[70] For each generated background, climate change uncertainty was evaluated by calculating the lower and upper bounds as two standard deviations below and above the mean of the 500 climate change impact results. For the endpoint impact categories, the probability of burden shifting was assessed by comparing the renewable syncrude or its derived products (naphtha, diesel, or kerosene; denoted as A) against the current business-as-usual scenario from ecoinvent (denoted as B). The probability of burden shifting, $P(A > B)$, represents the likelihood that A results in higher impacts than B, *i.e.*, worsening other categories while improving climate change performance. Burden shifting is considered to occur when $P(A > B) \geq 0.75$, whereas an impact reduction is indicated when $P(A > B) < 0.25$.

Table S19. Brief overview of the life cycle inventories (LCIs) used in this work, including the source and the activity name used in the dataset. The inventories used for the production each type of syncrude can be found in the subsequent tables.

Product	Scenario	Technology	Source
Hydrogen	CCU and hydrocracking	Wind-powered water electrolysis	D'Angelo *et al*.[71]
DAC CO_2	CCU	Direct air capture	Terlouw *et al.*[72]
Biomass agriculture	Biomass, agriculture	Wheat straw production	ecoinvent v3.10 ('straw production, stand-alone production')
Biomass forestry	Biomass, forestry	Birch tree production	ecoinvent v3.10 ('market for bundle, energy wood, measured as dry mass')
Biogas	Biogas	Biogas reforming	Istrate *et al.*[64]
Syncrude	Biomass, agriculture	Agricultural residue gasification, followed by the middle distillate synthesis (MDS)	This work
	Biomass, forestry	Forestry residue gasification, followed by the middle distillate synthesis (MDS)	This work
	Biogas	Bi-reforming of biogas, followed by the middle distillate synthesis (MDS)	This work
	CCU	DAC and PEM water electrolysis, followed by a RWGS reactor and the middle distillate synthesis (MDS)	This work
Crude oil	Fossil	Petroleum refining	ecoinvent v3.10 ('market for naphtha', 'market for kerosene', and 'market for diesel')

Table S20. LCI for syncrude from biomass (agricultural residues)

Functional unit: 1 kg of syncrude from biomass (agriculture)			
Input	**Amount**	**Unit**	**Database**
Straw production, stand-alone production	5.93	kg	ecoinvent 3.10
Hydrogen production, PEM electrolysis, green	0.01	kg	LCIs
Carbon dioxide storage and transport 200 km pipeline, storage 1000 m	5.80	kg	LCIs
Heat, district or industrial, natural gas	40.97	MJ	ecoinvent 3.10
Electricity, high voltage	2.20	kWh	ecoinvent 3.10
Output	**Amount**	**Unit**	**Database**
Syncrude, from wheat straw	1.00	kg	LCIs

Table S21. LCI for syncrude from biomass (forestry residues)

Functional unit: 1 kg of syncrude from biomass (forestry)			
Input	**Amount**	**Unit**	**Database**
Bundle, energy wood, measured as dry mass	5.52	kg	ecoinvent 3.10
Hydrogen production, PEM electrolysis, green	0.01	kg	LCIs
Carbon dioxide storage and transport 200 km pipeline, storage 1000 m	5.73	kg	LCIs
Heat, district or industrial, natural gas	22.94	MJ	ecoinvent 3.10
Electricity, high voltage	2.29	kWh	ecoinvent 3.10
Output	**Amount**	**Unit**	**Database**
Syncrude, from forestry residues	1.00	kg	LCIs

Table S22. LCI for syncrude from biogas

Functional unit: 1 kg of syncrude from biogas			
Input	**Amount**	**Unit**	**Database**
Market for biogas, sustainable feedstocks	3.54	m^3	ecoinvent 3.10
Cooling water	32.06	MJ	LCIs
Carbon dioxide storage and transport 200 km pipeline, storage 1000 m	2.41	kg	LCIs
Heat, district or industrial, natural gas	26.34	MJ	ecoinvent 3.10
Electricity, high voltage	0.65	kWh	ecoinvent 3.10
Output	**Amount**	**Unit**	**Database**
Syncrude, from biogas	1.00	kg	LCIs

Table S23. LCI for syncrude from carbon capture and utilisation (CCU)

Functional unit: 1 kg of syncrude from biomass (agriculture)			
Input	**Amount**	**Unit**	**Database**
Hydrogen production, PEM electrolysis, green	0.49	kg	ecoinvent 3.10
Carbon dioxide capture, from atmosphere, solid sorbents with heat pumps	2.91	Kg	LCIs
Cooling water	27.61	MJ	LCIs
Heat, district or industrial, natural gas	3.56	MJ	ecoinvent 3.10
Electricity, high voltage	0.37	kWh	ecoinvent 3.10
Output	**Amount**	**Unit**	**Database**
Syncrude, from CCU	1.00	kg	LCIs

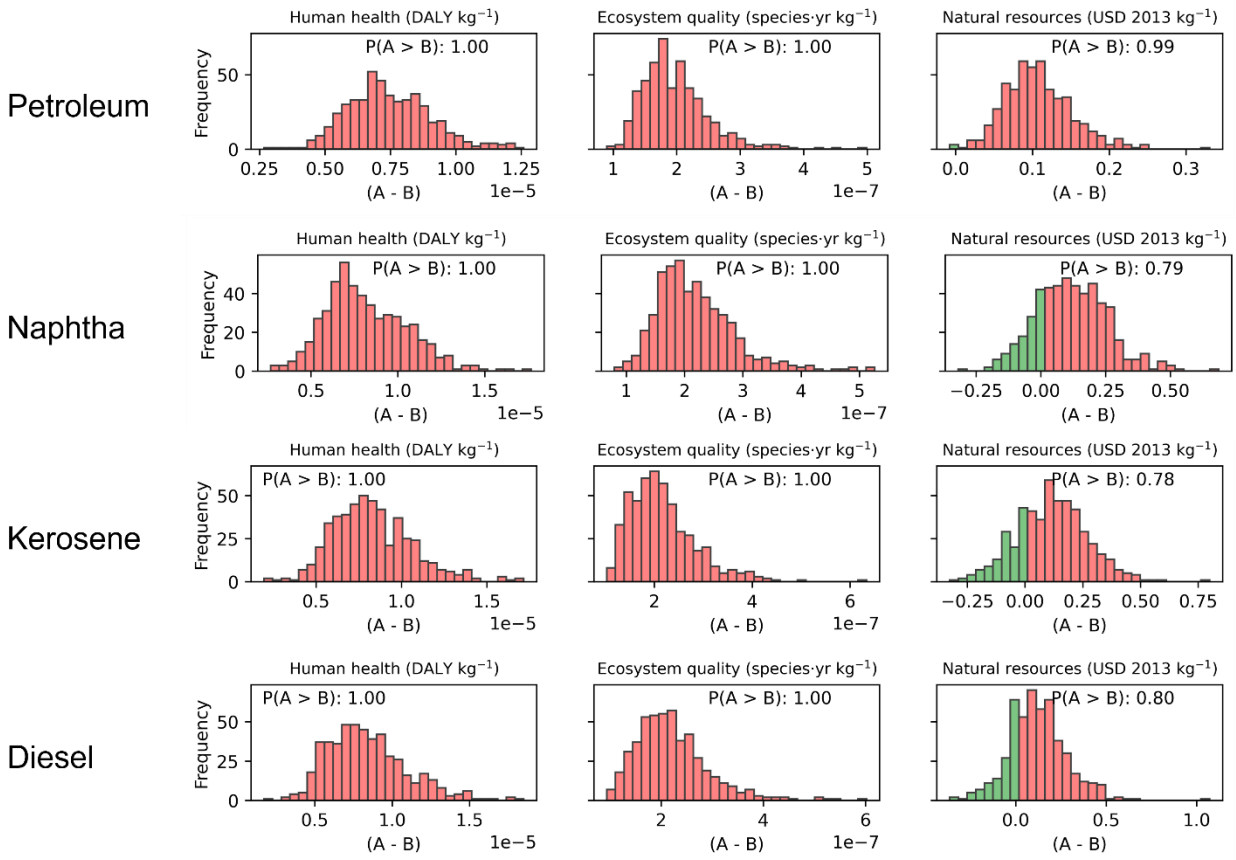

Fig. S9. Burden shifting Monte Carlo results for agricultural waste. The probability of burden shifting, P(A > B), represents the likelihood that the alternative green route A results in higher impacts than the standard fossil based one B, *i.e.*, worsening other categories while improving climate change performance. In this case, the burden shifting arises mainly from heat production that continues to use fossil feedstocks, contributing to higher natural resource impacts. The environmental impact results for naphtha, diesel, and kerosene were calculated using the refinery inventories from ecoinvent v3.10.

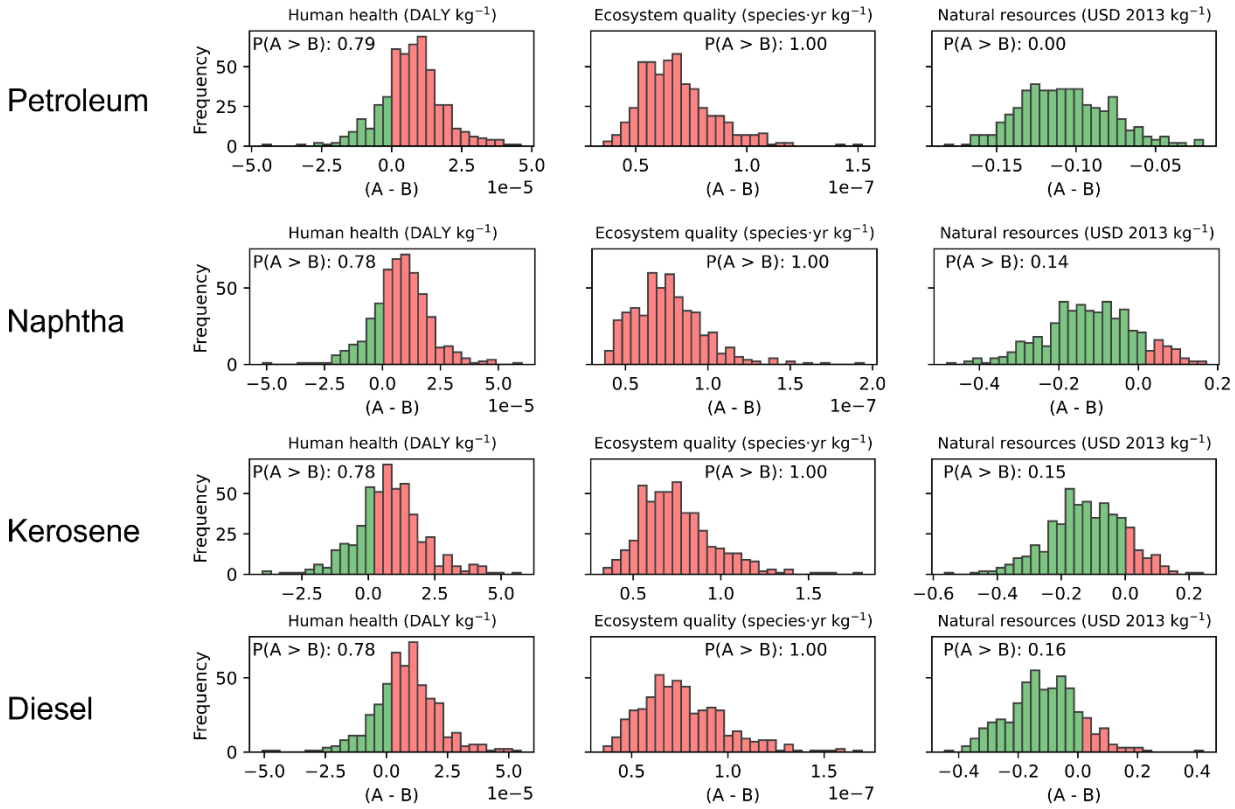

Fig. S10. Burden shifting results for forestry residues.

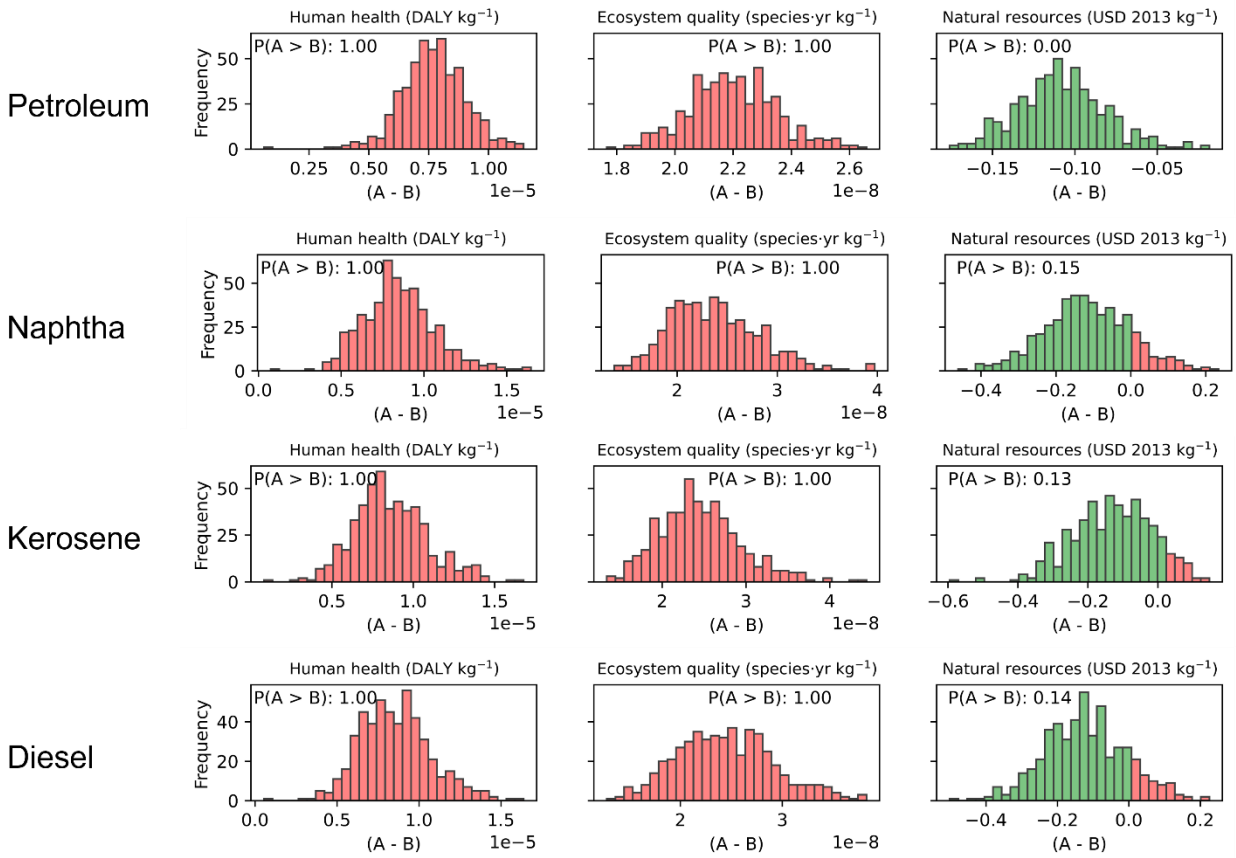

Fig. S11. Burden shifting results for biogas

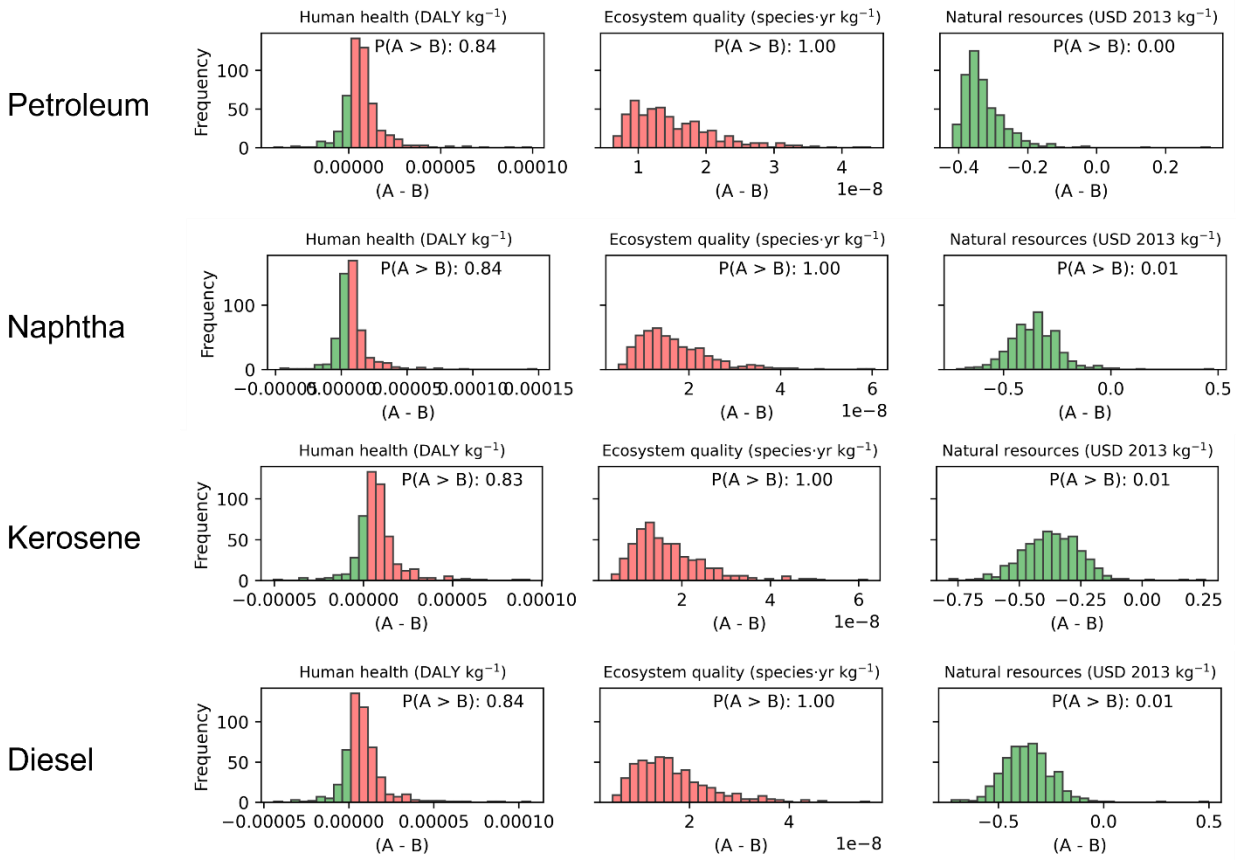

Fig. S12. Burden shifting results for CCU.

Table S24. Life cycle assessment results for the production of fossil crude and syncrude (cradle-to-gate) from different renewable feedstocks across three environmental impact categories: human health, natural resources, and ecosystem quality. The table highlights potential burden shifting and provides a broader analysis to the environmental impact of syncrude. The uncertainty of the values reported in this table has been assessed in the Monte Carlo analysis, shown in **Fig. S8** to **S11**.

Crude type	Human health [DALY. per kg]	Natural resources [$. per kg]	Ecosystem quality [species yr. per kg]
Fossil crude	$9.33 \cdot 10^{-7}$	$4.92 \cdot 10^{-1}$	$2.55 \cdot 10^{-9}$
Biogas	$7.98 \cdot 10^{-6}$	$3.62 \cdot 10^{-1}$	$2.28 \cdot 10^{-8}$
Forestry	$7.43 \cdot 10^{-6}$	$3.54 \cdot 10^{-1}$	$6.21 \cdot 10^{-8}$
Agriculture	$7.44 \cdot 10^{-6}$	$5.64 \cdot 10^{-1}$	$1.86 \cdot 10^{-7}$
CCU	$6.19 \cdot 10^{-6}$	$1.39 \cdot 10^{-1}$	$1.39 \cdot 10^{-8}$

7. Net-zero refinery syncrude blending

The final section employs a linear blending model between syncrude and fossil crude oil. For this purpose, a barrel of syncrude and a barrel of petroleum could be chosen equivalently, under the constraint of regional demand. For a given region *i*, the demand constraint was therefore defined by **Equation S9**. The optimisation was run using the Baron global optimiser in the Pyomo python package.[73,74] For each country, the model consisted of 7 variables and the CPU time per run was reported to be around 0.02 s.

$$D_i = \sum_j P_{i,j} + F_i \; \forall i \qquad \textbf{(Equation S9)}$$

where:

- D_i is the total demand in region i;
- $P_{i,j}$ the production quantity of syncrude from feedstock type j in region i;
- F_i the quantity of fossil crude oil chosen by the model in region i.

The model seeks to minimise cost and the emissions embodied in the blend. Two objective functions are, thus, defined, **Equations S10** and **S11**.

$$TC_i = \sum_j P_{i,j} \cdot \; TAC_{i,j} + F_i \cdot CF \quad \forall i \qquad \textbf{(Equation S10)}$$

where:

- TC_i is the total cost of the system in region i;
- $TAC_{i,j}$ is the cost per barrel of syncrude from feedstock type j in region i;
- $P_{i,j}$ the production quantity of syncrude from feedstock type j in region i;
- CF the cost of a barrel of fossil crude oil;
- F_i the quantity of fossil crude oil chosen by the model in region i.

$$TE_i = \sum_j P_{i,j} \cdot \; E_{i,j} + F_i \cdot EF \quad \forall i \qquad \textbf{(Equation S11)}$$

where:

- TE_i are the total emissions of the system in region i;
- $E_{i,j}$ is the cradle-to-gate emissions per barrel of syncrude from feedstock type j in region i;
- $P_{i,j}$ the production quantity of syncrude from feedstock type j in region i;
- EF the cradle-to-gate emissions of a barrel of fossil crude oil;
- F_i the quantity of fossil crude oil chosen by the model in region i.

As discussed in **Section S6**, the total GHG emissions (TE_i) were then normalised by the number of barrels produced to allow for an easy comparison between fossil and syncrude.

First, both cost and emissions were minimised separately, resulting in the extreme points. Then, the cost objective function was minimised under an upper emission constraint. By reducing the upper emission constraint further until its extreme point, this yielded a Pareto curve, as shown in **Fig. 5**. This procedure was

followed using **Equations S9**, **S10**, and **S11** for each region. The input parameters for each of the selected regions are listed in **Table S21**.

Table S25. Input parameters for the NZE blend optimisation. C_j represents the cost of a barrel of syncrude from feedstock type j, E_j the corresponding cradle-to-gate emissions for the same type of syncrude. The subscript f indicates the cost and emissions of fossil crude oil.

Parameter	Unit	Europe	North America	China	Russia	India	Brazil	South Africa	Japan
TAC_{biogas}	USD per bbl	98.3	64.3	96.3	66.0	104.3	139.9	106.2	140.2
E_{biogas}	kg CO_2-eq. per kg crude	-1.8	-1.8	-1.8	-1.8	-1.8	-1.8	-1.8	-1.8
$TAC_{agriculture}$	USD per bbl	158.4	99.8	151.0	104.8	161.4	220.6	167.9	235.0
$E_{agriculture}$	kg CO_2-eq. per kg crude	-3.7	-3.7	-3.7	-3.7	-3.7	-3.7	-3.7	-3.7
$TAC_{forestry}$	USD per bbl	100.5	62.6	92.5	67.5	96.6	133.2	103.4	153.6
$E_{forestry}$	kg CO_2-eq. per kg crude	-5.7	-5.7	-5.7	-5.7	-5.7	-5.7	-5.7	-5.7
TAC_{CCU}	USD per bbl	478.4	472.6	477.2	473.3	477.9	438.5	478.9	486.4
E_{CCU}	kg CO_2-eq. per kg crude	-0.9	-0.9	-0.9	-0.9	-0.9	-0.9	-0.9	-0.9
CF	USD per bbl	60.0	60.0	60.0	60.0	60.0	60.0	60.0	60.0
EF	kg CO_2-eq. per kg crude	0.8	0.8	0.8	0.8	0.8	0.8	0.8	0.8

References

1 S. P. Keller, Air Command and Staff College, 2011.

2 H. Schulz, *Applied Catalysis A: General*, 1999, 186, 3–12.

3 Celebrating our heritage |, https://www.sasol.com/celebrating-our-heritage, (accessed 14 August 2025).

4 The return of a classic to fuel production, https://www.mpg.de/511447/fischer-tropsch-synthesis-2005, (accessed 14 August 2025).

5 J. Eilers, S. A. Posthuma and S. T. Sie, *Catal Lett*, 1990, 7, 253–269.

6 Shell MDS Malaysia Celebrates 30 Years In Bintulu | About Us, https://www.shell.com.my/about-us/media/2024-press-releases/shell-mds-malaysia-celebrates-30-years-in-bintulu.html, (accessed 14 August 2025).

7 Pearl GTL | Shell Qatar, https://www.shell.com.qa/about-us/projects-and-sites/pearl-gtl.html, (accessed 14 August 2025).

8 M. Marchese, M. Gandiglio and A. Lanzini, *Front. Energy Res.*, 2021, 9, 773717.

9 M. Marchese, G. Buffo, M. Santarelli and A. Lanzini, *Journal of CO2 Utilization*, 2021, 46, 101487.

10 J. D. Medrano-García, M. T. Chagas and G. Guillén-Gosálbez, *ACS Sustainable Chem. Eng.*, 2025, 13, 7088–7097.

11 M. F. U. Hasnain, H. O. Ali, S. Aziz, P. M. Kouotou, M. Waqas, S. M. A. Naqvi, M. H. Athar, M. Ammar, I. Shah and D.-W. Jung, *Arabian Journal of Chemistry*, 2024, 17, 105821.

12 R. Istrate, A. Nabera, J. Pérez-Ramírez and G. Guillén-Gosálbez, *One Earth*, 2024, 7, 2235–2249.

13 G. A. Olah, A. Goeppert, M. Czaun, T. Mathew, R. B. May and G. K. S. Prakash, *J. Am. Chem. Soc.*, 2015, 137, 8720–8729.

14 A. Sodiq, Y. Abdullatif, B. Aissa, A. Ostovar, N. Nassar, M. El-Naas and A. Amhamed, *Environmental Technology & Innovation*, 2023, 29, 102991.

15 M. Bonanno, K. Müller, B. Bensmann, R. Hanke-Rauschenbach, D. Aili, T. Franken, A. Chromik, R. Peach, A. T. S. Freiberg and S. Thiele, *Advanced Materials Technologies*, 2024, 9, 2300281.

16 M. González-Castaño, B. Dorneanu and H. Arellano-García, *React. Chem. Eng.*, 2021, 6, 954–976.

17 J. E. Apolinar-Hernández, S. L. Bertoli, H. G. Riella, C. Soares and N. Padoin, *Energy Fuels*, 2024, 38, 1–28.

18 A. de Klerk, *Green Chem.*, 2008, 10, 1249–1279.

19 P. L. Perez, A. K. Gurnon, K. Chichak, J. McDermott, J. de Paulo, W. Peng and X. Xie, in *Offshore Technology Conference*, OnePetro, 2016.

20 Civil Aviation Fuel | Jet Fuel Specifications | Shell Global, https://www.shell.com/business-customers/aviation/aviation-fuel/civil-jet-fuel-grades.html, (accessed 5 November 2025).

21 EN 590 Diesel Fuel Specifications (ULSD), https://www.crownoil.co.uk/fuel-specifications/en-590/, (accessed 5 November 2025).

22 P. S. F. Mendes, J. M. Silva, M. F. Ribeiro, A. Daudin and C. Bouchy, *Catal. Sci. Technol.*, 2020, 10, 5136–5148.

23 R. Farhan Hussain, A. Mokhtari, A. Ghalambor and M. Amini Salehi, in *IoT for Smart Operations in the Oil and Gas Industry*, Elsevier, 2023, pp. 105–131.

24 Aspen HYSYS | Leading Process Simulation Software for Oil & Gas | AspenTech, https://www.aspentech.com/en/products/engineering/aspen-hysys, (accessed 1 December 2025).

25 L. Desport, A. Gurgel, J. Morris, H. Herzog, Y.-H. H. Chen, S. Selosse and S. Paltsev, *Energy Economics*, 2024, 129, 107244.

26 PricewaterhouseCoopers, Green hydrogen economy - predicted development of tomorrow, https://www.pwc.com/gx/en/industries/energy-utilities-resources/green-hydrogen-cost.html, (accessed 15 August 2025).

27 Global Energy Review 2020 – Analysis, https://www.iea.org/reports/global-energy-review-2020, (accessed 13 August 2025).

28 J. Huo, Z. Wang, P. Lauri, J. D. Medrano-García, G. Guillén-Gosálbez and S. Hellweg, *Environ. Sci. Technol.*, 2024, 58, 13748–13759.

29 IEA Bioenergy, *Sustainable potentials for renewable gas trade*, International Energy Agency, 2022.

30 B. E. Dale, S. Bozzetto, C. Couturier, C. Fabbri, J. A. Hilbert, R. Ong, T. Richard, L. Rossi, K. D. Thelen and J. Woods, *Biofuels, Bioproducts and Biorefining*, 2020, 14, 1335–1347.

31 S. Li, presented in part at the EUBCE, 2024.

32 F. B. Lueckel, M. Chanika, S. Majer, U. Fritsche, H. W. Gress, C. Boyce and R. Monaghan, *Synthesis Report of Work package 2 of the IEA Bioenergy Intertask project Renewable Gases: Deployment, markets and sustainable trade*, International Energy Agency, 2022.

33 A. Dey and R. C. Thomson, *Sustainable Energy Fuels*, 2022, 7, 209–241.

34 A. Freddo, F. Marques and K. Finco, *Brazilian Biogas Overview - 2021*, CIBiogás – Centro Internacional de Energias Renováveis - Biogás, 2021.

35 C. I. Marrison and E. D. Larson, *Biomass and Bioenergy*, 1996, 10, 337–351.

36 S. Yokoyama and Y. Matsumura, *J. Jpn. Inst. Energy*, 2015, 94, 1079–1086.

37 Refineries map, https://www.concawe.eu/refineries-map/, (accessed 16 August 2025).

38 S. V. Vassilev, D. Baxter, L. K. Andersen and C. G. Vassileva, *Fuel*, 2010, 89, 913–933.

39 P. Panja, B. McPherson and M. Deo, *Carbon Capture Science & Technology*, 2022, 3, 100041.

40 J. Frątczak, J. Górska, M. Babor, Z. Gholami, J. M. Hidalgo Herrador and H. de Paz Carmona, *Applied Sciences*, 2024, 14, 4656.

41 O. Onel, A. M. Niziolek, J. A. Elia, R. C. Baliban and C. A. Floudas, *Ind. Eng. Chem. Res.*, 2015, 54, 359–385.

42 G. Towler and R. Sinnott, Eds, *Chemical engineering design: principles, practice and economics of plant and process design*, Elsevier/Butterworth-Heinemann, Amsterdam Boston, 2008.

43 Useful Data Sets, https://pages.stern.nyu.edu/~adamodar/New_Home_Page/databreakdown.html, (accessed 29 July 2025).
44 Fluid Mechanics, https://www.training.itservices.manchester.ac.uk/public/gced/CEPCI.html?reactors/CEPCI/index.html, (accessed 29 July 2025).
45 A. Nabera, A. J. Martín, R. Istrate, J. Pérez-Ramírez and G. Guillén-Gosálbez, *Green Chem.*, 2024, 26, 6461–6469.
46 Sustainable supply potential and costs – Outlook for biogas and biomethane, https://www.iea.org/reports/outlook-for-biogas-and-biomethane-prospects-for-organic-growth/sustainable-supply-potential-and-costs, (accessed 16 August 2025).
47 Hay and straw prices | AHDB, https://ahdb.org.uk/dairy/hay-and-straw-prices, (accessed 16 August 2025).
48 BioBoost - Feedstock, potential, supply and logistics, https://www.bioboost.eu/results/feedstock_potential_supply_and_logistics.html, (accessed 16 August 2025).
49 Bulk Oxygen Price Trend, Index, Chart and Forecast, https://www.imarcgroup.com/bulk-oxygen-pricing-report, (accessed 27 February 2026).
50 Crude Oil - Price - Chart - Historical Data - News, https://tradingeconomics.com/commodity/crude-oil, (accessed 16 August 2025).
51 European Wholesale Electricity Price Data, https://ember-energy.org/data/european-wholesale-electricity-price-data, (accessed 13 August 2025).
52 Electricity Monthly Update - U.S. Energy Information Administration (EIA), https://www.eia.gov/electricity/monthly/update/print-version.php, (accessed 13 August 2025).
53 Electricity prices around the world, https://www.globalpetrolprices.com/electricity_prices/, (accessed 13 August 2025).
54 [nrg_pc_203] Gas prices for non-household consumers - bi-annual data (from 2007 onwards), https://ec.europa.eu/eurostat/databrowser/view/nrg_pc_203/default/table?lang=entat, (accessed 13 August 2025).
55 Gas and electricity prices in the non-domestic sector, https://www.gov.uk/government/statistical-data-sets/gas-and-electricity-prices-in-the-non-domestic-sector, (accessed 13 August 2025).
56 Natural gas prices around the world, December 2024, https://www.globalpetrolprices.com/natural_gas_prices/, (accessed 13 August 2025).
57 A. Nabera, I.-R. Istrate, A. J. Martín, J. Pérez-Ramírez and G. Guillén-Gosálbez, *Green Chem.*, 2023, 25, 6603–6611.
58 About Shell MDS in Bintulu, Sarawak | Business, https://www.shell.com.my/business/shell-middle-distillate-synthesis/about-smds.html, (accessed 13 August 2025).

59 R. Overtoom, N. Fabricius and W. Leenhouts, in *Proceedings of the 1st Annual Gas Processing Symposium*, eds H. E. Alfadala, G. V. Rex Reklaitis and M. M. El-Halwagi, Elsevier, Amsterdam, 2009, vol. 1, pp. 378–386.
60 Jobs from investment in green hydrogen. Update and extension, https://cedelft.eu/publications/jobs-from-investment-in-green-hydrogen/, (accessed 13 August 2025).
61 Direct Air Capture Workforce Development, https://rhg.com/research/direct-air-capture-workforce-development/, (accessed 13 August 2025).
62 Biomass to power, https://www.ceew.in/biomass-power, (accessed 13 August 2025).
63 A. Ganter, K. E. Lonergan, H. M. Büchi and G. Sansavini, *One Earth*, 2024, 7, 1981–1993.
64 R. Istrate, A. Nabera, J. Pérez-Ramírez and G. Guillén-Gosálbez, *One Earth*, 2024, 7, 2235–2249.
65 International Standards Organization, *In ISO 14040:2006 Environmental Management--Life Cycle Assessment--Principles and Framework*, 2006.
66 International Standards Organization, *In ISO 14044:2006 Environmental Management--Life Cycle Assessment--Requirements and Guidelines*, 2006.
67 E. Lucas, A. J. Martín, S. Mitchell, A. Nabera, L. F. Santos, J. Pérez-Ramírez and G. Guillén-Gosálbez, *Green Chem.*, 2024, 26, 9300–9309.
68 Intergovernmental Panel on Climate Change (IPCC), *Climate Change 2021 – The Physical Science Basis: Working Group I Contribution to the Sixth Assessment Report of the Intergovernmental Panel on Climate Change*, Cambridge University Press, 1st edn., 2023.
69 M. A. J. Huijbregts, Z. J. N. Steinmann, P. M. F. Elshout, G. Stam, F. Verones, M. Vieira, M. Zijp, A. Hollander and R. van Zelm, *Int J Life Cycle Assess*, 2017, 22, 138–147.
70 E. A. Groen, R. Heijungs, E. A. M. Bokkers and I. J. M. de Boer, *Environmental Modelling & Software*, 2014, 62, 316–325.
71 S. C. D'Angelo, S. Cobo, V. Tulus, A. Nabera, A. J. Martín, J. Pérez-Ramírez and G. Guillén-Gosálbez, *ACS Sustainable Chem. Eng.*, 2021, 9, 9740–9749.
72 T. Terlouw, K. Treyer, C. Bauer and M. Mazzotti, *Environ. Sci. Technol.*, 2021, 55, 11397–11411.
73 W. E. Hart, J.-P. Watson and D. L. Woodruff, *Math. Prog. Comp.*, 2011, 3, 219–260.
74 A. Khajavirad and N. V. Sahinidis, *Math. Prog. Comp.*, 2018, 10, 383–421.